Spherical harmonic decomposition applied to spatial-temporal analysis of human high-density electroencephalogram

B. M. Wingeier*
Brain Sciences Institute, Swinburne University of Technology, 400 Burwood Road, Hawthorn, Victoria 3122, Australia

P. L. Nunez
Department of Biomedical Engineering, Boggs Center, Tulane University, New Orleans, Louisiana 70118

R. B. Silberstein
Brain Sciences Institute, Swinburne University of Technology, 400 Burwood Road, Hawthorn, Victoria 3122, Australia

(Received 2 November 2000; revised manuscript received 4 June 2001; published 26 October 2001)

We demonstrate an application of spherical harmonic decomposition to the analysis of the human electroencephalogram (EEG). We implement two methods and discuss issues specific to the analysis of hemispherical, irregularly sampled data. Spatial sampling requirements and performance of the methods are quantified using simulated data. The analysis is applied to experimental EEG data, confirming earlier reports of an approximate frequency–wave-number relationship in some bands.

DOI: 10.1103/PhysRevE.64.051916 PACS number(s): 87.80.Tq, 02.30.Px, 87.19.La,

I. INTRODUCTION

The human electroencephalogram (EEG), as measured at the scalp, represents a superposition of electric fields resulting from post-synaptic potentials in neocortex, the thin (2 to 5 mm) surface layer of human brains. Several models of neocortical dynamics treat EEG as a mixed global/local phenomenon [1–3], and a better understanding of its spatial-temporal dynamics is necessary for evaluation and refinement of these models. Its temporal behavior has been studied at length, both by clinical observation [4] and with such tools as power spectra [5], coherence [6], the Hilbert transform [7], and many others. However, until recently poor spatial resolution (due to minimal electrode sampling and under use of head models) has limited spatial analysis of EEG [1,2,8].

As a potential field on a near-hemispherical surface, EEG is amenable to analysis by spherical harmonic decomposition. In this paper, we apply two methods of decomposition (one described by Cadusch *et al.* [9] and one adapted from Misner [10]) to 131-channel EEG data. Using simulated data, we discuss issues and pitfalls relevant to such an analysis, specifically the effect of integration over a hemisphere, limited sampling density, and deviations from a spherical surface. The adapted Misner decomposition (described fully in the Appendix) is applied to experimental data. From this application, we draw preliminary conclusions regarding the frequency–wave-number relation of neocortical activity.

II. CONSIDERATIONS FOR DECOMPOSITION OF EEG

We use the real spherical harmonics [11], defined on the sphere Ω and described by the orthogonality integral

$$\langle Y_{lm}|Y_{l'm'}\rangle = \int_0^{2\pi}\int_0^{\pi} Y_{lm}(\theta,\phi)Y_{l'm'}(\theta,\phi)\sin\theta d\theta d\phi = \delta_{l,l'}\delta_{m,m'}. \quad (1)$$

In theory, a potential field $\Phi(\Omega)$ may be decomposed into spherical harmonic amplitudes Φ_{lm} defined by

$$\Phi_{lm} = \int_\Omega Y_{lm}(\theta,\phi)\Phi(\theta,\phi)d^2\Omega. \quad (2)$$

In practice, where $\Phi(\Omega)$ is sampled at discrete locations Γ, we would prefer to accomplish the decomposition in the form

$$\hat{\Phi}_{lm} = \sum_{x\in\Gamma} \mu_{lm}(x)F(x), \quad (3)$$

where the $\hat{\Phi}_{lm}$ are estimates of Φ_{lm}, which may be implemented in a single matrix multiplication if the $\mu_{lm}(x)$ are constant for a given sampling grid Γ. The transition from theory to practice, however, may be complex. In the case of EEG or similar data, we encounter three major and two minor issues.

A. Discretization and regularization

First, with discretely sampled data $F(\Gamma)$, Eqs. (1) and (2)—both defined over a continuous medium—must be used with care. Even with appropriate sampling densities (see *Sampling*, below), discretization of the inner product of Eq. (1) invalidates the orthogonality relation. Note that the fundamental ability of orthogonal functions to represent sampled signals is not compromised. Rather, the decomposition becomes more difficult as a given signal may be approximately reconstructed with more than one l,m spectrum. Blind application of a discretized Eq. (2) may yield an accurate reconstruction at the sample points, but with large artifacts in the higher spatial frequencies. The apparently accurate reconstruction will often be due to an unrealistic superposition of high-amplitude, high-frequency modes.

We must invoke constraint or regularization techniques to address this issue. Recently, Misner [10] introduced a regu-

*Also at Department of Biomedical Engineering, Tulane University, New Orleans, LA 70118; email address: wingeier@bsi.swin.edu.au

larization method for decomposition on a rectangular three-dimensional grid; that is, generalized to use $Y_{nlm}(r,\theta,\phi)$. We describe here the special case of sampling on a spherical surface, more relevant to EEG analysis, in which r is constant. In Misner's method, a matrix G_{AB} represents the discretized inner product

$$G_{AB}=\langle Y_A|Y_B\rangle=\sum_{x\in\Gamma} Y_A(x)Y_B(x)w_x, \tag{4}$$

where A and B refer to index groups (lm). (For application to EEG, we use the real harmonics and replace Misner's weight function w_x with the effective area of each electrode.) Misner demonstrates that the mean square error due to discretization is minimized (the regularization constraint) by choosing

$$\mu_{lm}(x)=Y^{lm}(\theta,\phi)w_x, \tag{5}$$

for $x\in\Gamma$, where the ''adjoint spherical harmonics'' Y^B are defined as

$$Y^B=\sum_A Y_A(G_{AB})^{-1}. \tag{6}$$

The coefficients μ_{lm} remain constant for a given sampling grid, and may be used in Eq. (3) to estimate Φ_{lm}.

In a separate analysis, Cadusch *et al.* [9] approached the problem as a side issue of spherical spline interpolation of the EEG. Adapted to the notation used here, the second-order spline fit Φ' over the sphere Ω is given by

$$\Phi'(\Omega)=d+\sum_{l=1}^{\infty}\sum_{m=-l}^{l}\left[\frac{l}{[l(l+1)]^2}\sum_{x\in\Gamma}c_xY_{lm}(x)\right]Y_{lm}(\Omega), \tag{7}$$

where the c_x and d are coefficients calculated from the sampled potentials. Equation (7) is equivalent to a spherical harmonic expansion of Φ', in terms of coefficients Φ_{lm} indicated by the bracketed term. Regularization is accomplished in this case by the spline fit, which is constrained to produce the smoothest approximation consistent with the sampled data. The spherical harmonic expansion coefficients Φ'_{lm}, then, are given by

$$\Phi'_{lm}=\begin{cases} d, & l=0; \\ \dfrac{1}{[l(l+1)]^2}\displaystyle\sum_{x\in\Gamma}c_xY_{lm}(x), & l\geq 1. \end{cases} \tag{8}$$

Using Cadusch *et al.*'s derivation of spline coefficients c_x and d, a constant matrix of μ_{lm} may be derived for each sampling grid, and used in Eq. (3) as discussed previously. Further detail on the spline fit may be found in the Ref. [9].

B. Hemispherical sampling

Particularly relevant to EEG analysis is the ambiguity introduced by sampling over only half of the sphere. For instance, the function Y_{10} is indistinguishable over the upper hemisphere from a sum of Y_{00} and several higher harmonics. In other words, the spherical harmonics Y_{lm} are no longer orthonormal for $0\leq\theta\leq\pi/2$; this may be expressed by replacing the δ in Eq. (1) with an error quantity ϵ

$$\langle Y_A|Y_B\rangle=\int_0^{2\pi}\int_0^{\pi/2}Y_A(\theta,\phi)Y_B(\theta,\phi)\sin\theta\,d\theta\,d\phi=\epsilon_{AB}. \tag{9}$$

In general, our hemispherical estimates $\hat{\Phi}'_A$ will be related to the hypothetical full-sphere result by the matrix of ϵ_{AB}'s

$$\hat{\Phi}'=\boldsymbol{\epsilon}\hat{\Phi}. \tag{10}$$

It is impossible to calculate a more accurate result, by inversion of $\boldsymbol{\epsilon}$, for two reasons. First, the matrix $\boldsymbol{\epsilon}$ is ill conditioned ($R>10^8$, where the two-norm condition number R is the ratio of the largest singular value of $\boldsymbol{\epsilon}$ to the smallest) and thus, the inversion is problematic. More fundamentally, since the spherical harmonics are not truly orthogonal over the hemisphere, the matrix $\boldsymbol{\epsilon}$ expresses an unavoidable ambiguity between certain Y_{lm}.

Given this ambiguity, we must consider whether the spherical harmonics are the most appropriate set of basis functions for decomposition over the hemisphere. In the field of computer graphics, a hemispherical mapping of the Zernike polynomials (orthonormal over the unit disk) was proposed by Koenderink *et al.* [12] to represent the variance of reflectance over the hemisphere. However, the Zernike-based method provides no such convenient measure of spatial spectrum, independent of coordinate orientation, as is given by the collapsed-m angular power spectrum estimate described in Sec. II D.

Furthermore, we note that the underlying biological system (the human cortex) is not limited to the single hemisphere accessible to scalp electrodes. For this reason, the Y_{lm} may provide a better connection to brain anatomy and global-dynamic theory. For instance, the global alpha rhythm postulated in [1] and [2] would be a fundamental-mode oscillation over the entire cortex, analogous to the Y_{10} harmonic. Thus, the spherical harmonics seem appropriate for EEG analysis, when used with an understanding of the hemispherical error.

C. Sampling

Of course, when attempting to decompose experimental data, we must sample $\Phi(\Omega)$ at specific locations Γ. Assuming near-regularly spaced electrodes, our maximum resolvable l is determined by a spherical analog of the familiar time-domain Nyquist limit [13] $f_{\max}=1/(2\Delta T)$, where the maximum resolvable frequency $f_{\max}$ is determined by the sampling interval ΔT. For spatial sampling on a spherical surface, we replace ΔT with the analogous quantity γ, representing mean angular distance between adjacent electrodes. Since the l index indicates cycles per circumference (as well as the number of nodal lines across the sphere), we multiply by 2π to give a limit of $l_{\max}=\pi/\gamma$. In practice, sampling will degrade for frequency components under but near the Ny-

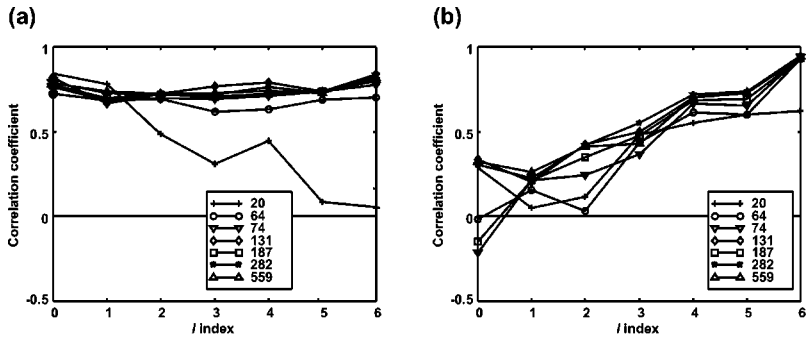

FIG. 1. Correlations between actual and estimated l power for uniformly distributed random spectra. Five hundred potential maps were generated from known wave-number spectra, with random power in each l component, uniformly distributed between 0 and 1. For each of seven electrode densities, wave number spectra were estimated by spherical harmonic decomposition of the 500 sampled maps. Correlations between actual power and estimated power were calculated over the 500 trials for each l component. Shown here for (a) adjoint harmonic and (b) spline methods, these correlations are a measure of the quality of a single decomposed power spectrum.

quist limit, so a practical limit of $f_{\max}=1/(3\Delta T)$ or $f_{\max}=1/(4\Delta T)$ is generally chosen. Likewise, here we adopt a conservative limit of

$$l_{\max}=\left[\frac{\pi}{2\gamma}\right], \tag{11}$$

or $l_{\max}=6$ using $\gamma=0.24$ for our 131-channel electrode cap. Note that the usual step of analog prefiltering (to avoid aliasing of higher frequencies) is not required here due to the low-pass characteristics of the head volume conductor [14].

D. Coordinate orientation

In many problems, the sphere has no preferred direction. The m indices are usually collapsed [15] to produce an angular power spectrum estimate $\hat{G}(l)$ as a function of wave number only

$$\hat{G}(l)=\sum_{m=-l}^{l}(\hat{\Phi}'_{lm})^2, \tag{12}$$

which is independent of coordinate system orientation. As well, in the simulations of Sec. III, we found the ''hemispherical error'' in l spectrum to be independent of orientation. In some EEG studies, of course, the orientation of the underlying cerebral hemispheres may be relevant. In such cases, local spatial Fourier analysis [1] should adequately complement our decomposition without the complication of distinguishing m modes.

E. Nonspherical media

We assume that our medium Ω is a sphere, whereas biological data is often sampled on an irregular surface. The upper surface of the ''average'' human head [16] may be represented as a hemiellipsoid with axes $a=10.52$ cm, $b=7.66$ cm, and $c=8.41$ cm, or alternatively 25, -9, and 0% elongation from a perfect sphere. Although prolate spheroidal harmonics have been applied to biophysical field problems [17–19], the technique is often unwieldy. In comparison to error from ϵ_{AB}, especially for low l, we assume the error due to approximating the ellipsoidal surface with a spherical surface is negligible.

III. APPLICATION TO SIMULATED DATA

We generated evenly tessellated, hemispherical electrode maps of 74, 187, 282, and 559 electrodes, in addition to common experimental maps of 20, 64, and 131 [8] electrodes. Five hundred potential maps were simulated for each electrode configuration. Each potential map was randomly generated with harmonics of up to degree $l=6$, such that the Φ_{lm} varied with uniform distribution between 0 and 1. Power-spectrum estimates $\hat{G}(l)$ were then calculated for each map, using both methods. Figure 1 shows Pearson's correlation coefficients r_l, calculated between $G(l)$ and $\hat{G}(l)$ over the 500 trials for each electrode map.

We have noted that the error due to ϵ_{AB} causes power from one (l,m) component to be misinterpreted as power in another, often of different l. Therefore, we might expect either method's performance to depend on the l spectrum being analyzed. Using preliminary experimental data, we constructed an approximate power spectrum $G_{norm}(l)$ for average-referenced scalp EEG, peaked at $l=1$ and $l=2$, and decaying with l^{-1} thereafter. Another five hundred potential maps were generated, with Φ_{lm} uniformly distributed between

$$0<\Phi_{lm}<\frac{G_{norm}(l)}{2l+1} \tag{13}$$

to simulate a physiologically realistic distribution of l spectra. Power spectrum estimates $\hat{G}(l)$ were calculated for each map using both methods. Results are shown in Fig. 2.

In general, results for the spline method—though often quite accurate—were dependent on the distribution of l spectra being measured, exact electrode positions, and electrode numbers. Results for the adjoint harmonic method appeared more robust, even for sparse $(n=64)$ sampling, although accuracy was somewhat less in the higher harmonics.

In both methods, for $l=6$, we observed minimal improvement for more than 131 electrodes. We thus believe that our

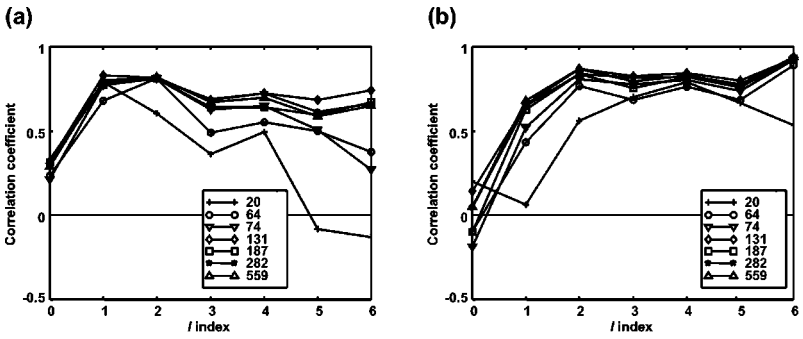

FIG. 2. Correlations between actual and estimated l power for more realistically distributed random spectra based on genuine EEG data. As in Fig. 1, but in original spectra, random power in each l component is uniformly distributed between 0 and $(2l+1)^{-1}$.

131-channel sampling is an appropriate tool for further study. Furthermore, given the limit in Eq. (11) and the known volume-conductor attenuation of higher modes [14], we suggest that the study of spatial frequencies higher than approximately $l=8$ will be better served by intracranial EEG than by denser electrode maps.

In general, for low l, the adjoint harmonic method seemed more consistent. We examined typical 131-channel decompositions (Fig. 3) to investigate further. Both methods accurately reproduced the potential maps ($r>0.9$ for 131 channels). The spline method, however, was slightly unstable for low l, and the erroneous negative $\hat{\Phi}_{lm}$ are reflected in the power spectrum.

IV. REFINEMENTS AND ANALYSIS OF ERROR

Any application of the spherical harmonic decomposition should take into account the estimated relative contribution of various error sources. Aside from measurement and experimental error, these may be divided into three categories: sampling error, orientation error, and hemispherical error.

A. Sampling error

Figures 1 and 2 indicate minimal improvement for $l\leqslant 6$ with more than 131 electrodes. We can thus deduce that the Nyquist-like limit in Eq. (11) is an appropriate guideline. When using coarser sampling, we expect some decrease in

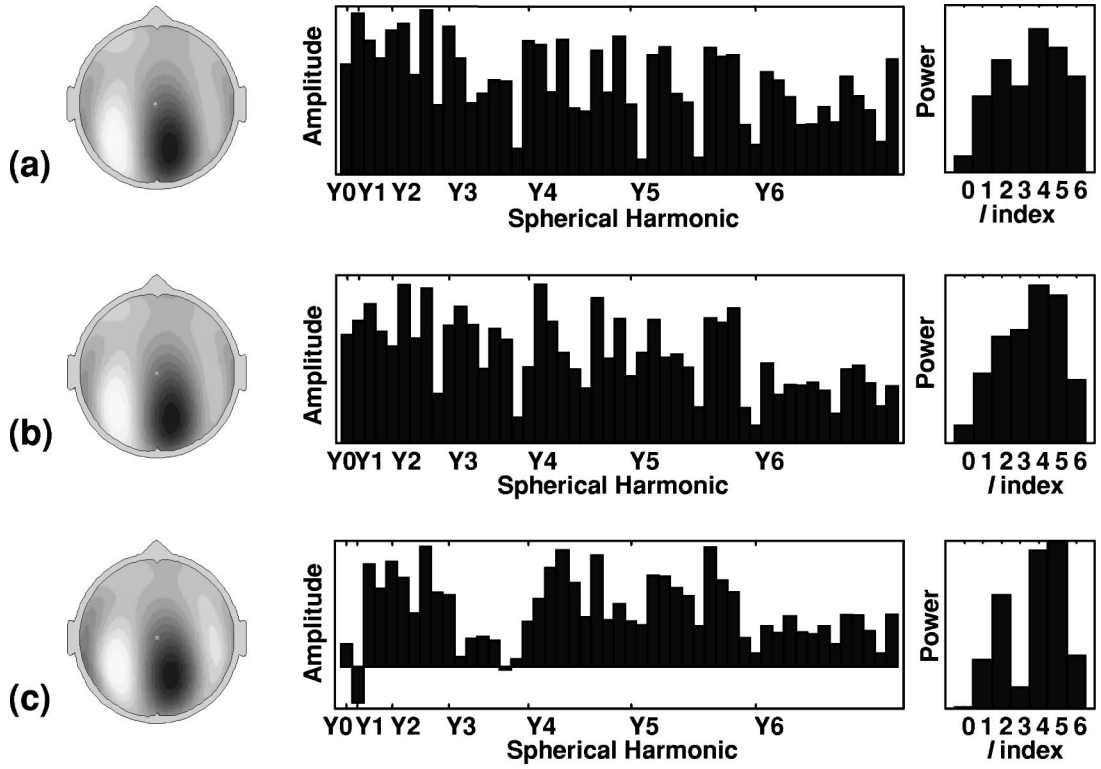

FIG. 3. Scalp topography (left column), l,m spectra (center column), and l power (right column) for a typical 131-channel spherical harmonic decomposition. The original map, shown in (a), represents a randomly generated l spectrum, randomly distributed through the m indices. The adjoint harmonic method (b) reconstructs topography and gives an approximation of l spectrum. Although the spline method (c) also reconstructs potential topography, we observe irregularities in the lower l amplitude estimates that contribute to decreased performance for these wave numbers, and a less accurate l-spectrum estimate. Amplitude values (center column) are expressed in μV. l power is expressed in $(\mu\mathrm{V})^2$, and is generated from l,m spectra using Eq. (12).

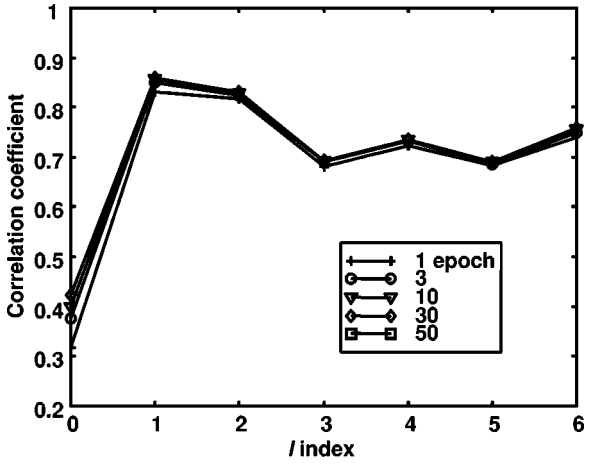

FIG. 4. Correlations between actual and estimated l power for multiple-epoch, adjoint-harmonic estimates of the same l spectrum, with epochs varying only in m component. For a reasonably isotropic and dense sample array, such as the 131-channel EEG grid used here, there is little orientation error, and thus, little improvement in results.

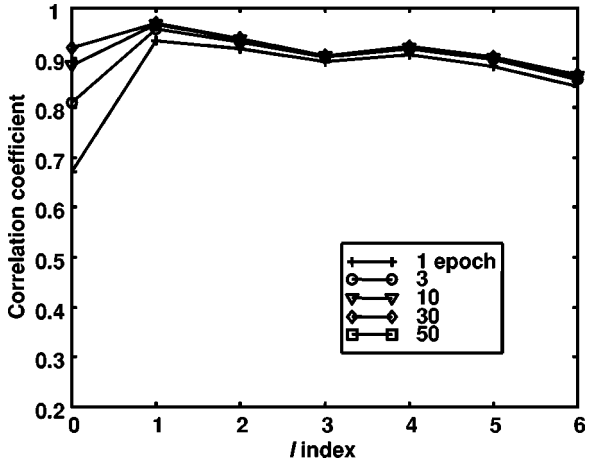

FIG. 5. Sampling a full sphere with 262 channels and the adjoint harmonic method, correlations between actual and estimated l power are shown for multiple-epoch (varying only in m component) estimates of the same l spectrum. By sampling over the full sphere, we eliminate hemispherical errors illustrated in Fig. 4. Remaining errors are due to orientation (note improvement with multiple epochs) and imperfect sampling.

performance for higher l. Decreased accuracy for 20, 64, and 74 channels (seen in Figs. 1 and 2, particularly for 20 channels) may be attributed to sampling error.

B. Orientation error

For a given l spectrum, results will vary if power is randomly distributed across the m's; that is, various m components interact differently with our hemispherical sample grid. Five hundred random l spectra, with realistic distribution of $G(l)$, were generated. Thirty 131-channel maps, randomly varying in m power, were generated for each original l spectrum. Figure 4 displays the resulting accuracy, again shown as correlation coefficient r_l between $G(l)$ and $\hat{G}(l)$ over the 100 trials.

Very little is gained in this simulation by decomposition of multiple epochs. As described in the following section, error due to m distribution of power is largely swamped by hemispherical error. In practice, however, we must emphasize (in the presence of random measurement noise) the importance of averaging decompositions across many epochs. Orientation error will also become significant if our sampling grid is severely nonuniform.

C. Hemispherical error

In Sec. II above, we have discussed the hemispherical error ϵ_{AB}. Although it is impossible to improve our decomposition results by inverting the matrix $\boldsymbol{\epsilon}$, we may generate a corresponding matrix for the power-spectrum result and use it to estimate the contribution of hemispherical error.

Power in a single harmonic $Y_{lm}(\theta,\phi)$ is blurred by the hemispherical decomposition into surrounding harmonics. Using the 131-channel sampling map, we generated five hundred potential maps for each of $l=0,\ldots 6$, each with one unit power distributed randomly among the available m's. By averaging over the five hundred resulting power spectra, for each l, we obtained an empirical ''averaged blurring matrix'' $\mathbf{E}$ for power spectra obtained from hemispherical decomposition. That is,

$$\hat{G}(l)\approx \mathbf{E}G(l). \tag{14}$$

The typical $\mathbf{E}$ for both methods is a blurred identity matrix; that is, error in power spectra is largely between adjacent l. Most $\mathbf{E}$ are invertable, and thus it may seem appropriate to deblur our spectra and calculate a more accurate result. However, we found that for realistic spectra, the benefit was marginal at best; as predicted in Sec. II, the error expressed by $\mathbf{E}$ was unavoidable.

Instead, $\mathbf{E}$ may be used to better understand the implications of hemispherical error. We calculated correlation coefficients as in Fig. 4, between $\mathbf{E}G(l)$ and $\hat{G}(l)$ over the 500 trials of 30 epochs for 131 electrodes. The resulting higher correlations (although not applicable to a decomposition of real data) are plotted in Fig. 5. By comparison with Figs. 2(a) and 4, the result indicates the importance of hemispherical error. In particular, after examination of typical $\mathbf{E}$ and $\boldsymbol{\epsilon}$ matrices, we may interpret the decreased performance at low l as blurring between adjacent wave numbers. Furthermore, the increased effect, seen in Fig. 5, of averaging across various m distributions indicates that some abrupt changes in performance may be attributed to sensitive interactions between $\mathbf{E}$ blurring and random m distribution.

Practically, the near-identity character of $\mathbf{E}$ is extremely useful. Hemispherical error manifests as blurring between adjacent l. Thus, we may expect composite measures such as the sum of power in $l=0,\ 1$ to be substantially more accurate than individual estimates. Figure 6 displays the accuracy of $l=0,\ 1$ and $l=2,\ldots,6$ adjoint harmonic power estimates (used below in our experimental trials), for 500 epochs, realistic l distribution, and various sampling densities.

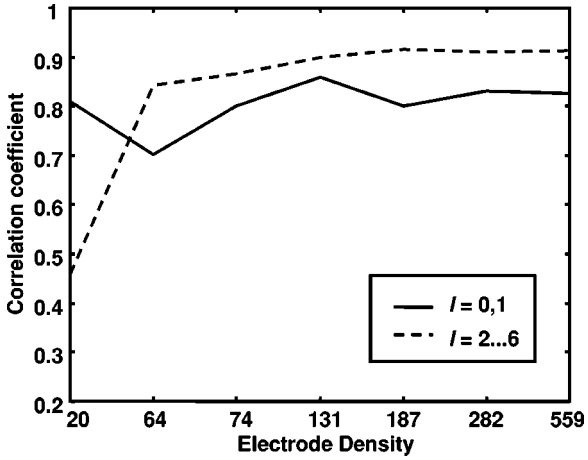

FIG. 6. Correlation coefficients, using the adjoint harmonic method, obtained by comparisons of estimated to actual summed power measures. The solid line represents power in $l=0$ and $l=1$ modes, and the broken line represents power summed over modes $l=2$ through $l=6$. Increased accuracy (as compared to part A of Fig. 2) is because most hemispherical error manifests as blurring between power in adjacent l's.

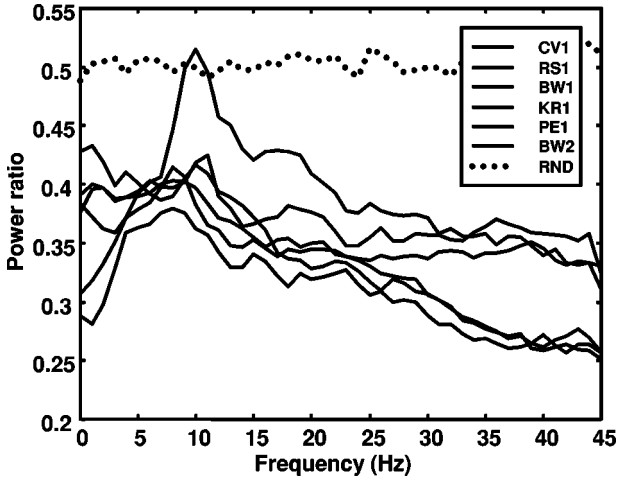

FIG. 7. Five to ten minutes of resting, eyes-closed EEG were collected with 131 channels from each of six subjects (one duplicated). Complex temporal Fourier coefficients were calculated for one-second epochs and subjected to spherical harmonic spatial decomposition using the adjoint harmonic method. Resulting wave number spectra were averaged for each 1 Hz band over the 300 to 600 epochs. The ratio of power in $l=0,1$ to $l=2,\ 3,\ 4,\ 5,\ 6$ is plotted as a simple indicator of a bias toward higher-spatial frequencies at higher-temporal frequencies (greater than about 10 Hz). This result is qualitatively consistent with the postulated existence of an approximate EEG dispersion relation, perhaps with alpha rhythm (8–13 Hz) representing the fundamental and lower overtones. A surrogate signal (dotted line), composed of random EEG-like noise and subjected to the same analysis, showed no such relation.

V. APPLICATION TO EXPERIMENTAL DATA

Nunez in 1974 [20,21], using Fourier analysis, observed a relationship between spatial and temporal frequency roughly consistent with simple wave dispersion relations. Crude wave-number spectra were approximately determined from eight bipolar channels evenly spaced along the (sagittal) midline. The ratio of power at wave-number 0 to power at higher wave numbers was shown to decrease consistently with temporal frequency in the range 8 to 13 Hz. Later, Shaw [22] estimated high– and low–wave-number components by comparing EEG sampled at 2 cm electrode spacing with aliasing in EEG sampled at 5 cm spacing. Shaw's aliasing index, indicating the relative contribution of high–wave-number power, was least in the alpha band and increased consistently from 10 to 30 Hz in all four subjects.

We attempted to reproduce these results in order to test the adjoint harmonic method under experimental conditions. We analyzed 131-channel EEG (resting, eyes closed) in five human subjects. Temporal Fourier coefficients were determined for 300 to 600 one-second epochs (depending on available data), and l spectra averaged over these epochs.

Results are summarized in Fig. 7 as the ratio of power in low ($l=0,\ 1$) to power in high- ($l=2,\ 3,\ 4,\ 5,\ 6$) spatial frequencies. Above approximately $f=8$ Hz, with increasing f, we observed a general trend towards power in higher l. We also observed high–wave-number power in the delta band ($f\leqslant 3$ Hz). The alpha band (c. 8–13 Hz) was characterized by the highest power in low spatial frequencies.

In order to rule out methodological artifact, we generated and analyzed 300 seconds of simulated EEG using 3602 uncorrelated sources, each generating 1/f noise through a head volume conductor model as described in [14]. As expected, the EEG-like noise (labeled RND in the figure) showed no relation between spatial and temporal frequencies.

VI. CONFIDENCE INTERVAL ESTIMATION

Estimates of the temporal power spectrum are known to vary in chi-square distribution, assuming normally distributed estimates of the underlying Fourier coefficients [13]. The error distribution for spatial spectrum estimates, on the other hand, is complicated by the dependence of hemispherical and orientation error on the entire l spectrum. For composite measures of both spatial and temporal spectra, such as shown in Fig. 7, the situation becomes even more problematic. We propose an empirical test for estimation of such confidence levels. The method is analogous to the randomization tests commonly applied in nonparametric statistical analysis; further detail regarding such tests may be found in [23].

Let

$$A=\frac{G_{01}}{G_{2,\ldots,6}}, \tag{15}$$

where G_{01} is the total power in harmonics $l=0$ and $l=1$, and $G_{2,\ldots,6}$ is the total power in harmonics $l=2$ through $l=6$. Let $\hat{G}_{01}$, $\hat{G}_{2,\ldots,6}$, and $\hat{A}$ represent estimates of the same. In Sec. V, we calculated $\hat{A}_f$ in EEG data for various temporal frequencies. Here, we calculate an approximate 95% confidence interval for single-epoch estimates of the actual A_f. The confidence interval will apply only to the spatial spectrum composite measure, neglecting error (or

nonstationarity) in temporal frequency spectra, which for many applications may be as important. Note, though, that for 300 epochs the normalized standard error of a temporal power spectrum estimate is less than 6%.

To determine an empirical confidence interval, one would typically examine the distribution of random resamples. In the current application, we created many random l spectra from an estimated distribution of l power, simulated many decompositions, and examined the resulting distribution as follows.

Since hemispherical error is dependent on l spectrum, the result will be influenced by the distribution of the random spectra. An approximate distribution of l power must be assumed in order to calculate the confidence interval. Srinivasan *et al.* [14] analytically estimated the spatial frequency domain transfer function for volume-conduction blurring of scalp potential as proportional to $(2l+1)^{-1}$. This ''spatial smearing'' is due mainly to the poorly conducting skull and physical separation between cortical current sources and scalp electrodes. Unless a more specific distribution is justified by theoretical or physiological considerations, a uniform or chi-square distribution, scaled by $(2l+1)^{-1}$, and with this power randomly distributed through the m indices, is an appropriate and conservative assumption. In practice, we have found that the confidence interval estimate is not sensitive to small changes in the assumed distribution.

In this calculation, therefore, we assumed that power in each bin of the underlying l spectra varies in uniform distribution in proportion to $(2l+1)^{-1}$, and that with average-referenced data the contribution of $l=0$ is negligible. A large number (20 000) of l,m spectra were generated, randomly selecting for each l bin a value from the appropriate distribution. The decomposition was performed, and the composite measure A calculated, for each randomized spectrum.

By examining the distribution of known surrogate A_{rand}, which produce a certain estimate $\hat{A}_{rand}$, we can estimate an empirical confidence interval for our spectral estimate. In Fig. 8, we show the scatter plot of A_{rand} against $\hat{A}_{rand}$ with 95% confidence intervals. For a given estimate $\hat{A}$ and the assumptions discussed above, 95% of the time, the actual A will fall between the two lines shown.

A similar procedure may be used to calculate confidence intervals for other estimates, whether the actual G_l or other composite measures. In summary, a large number of l,m spectra must be generated from a conservatively broad assumed power distribution. The corresponding scalp maps are decomposed; the estimate of interest is calculated for each and plotted against those calculated from the original spectra. Confidence intervals, then, are the vertical limits between which the actual value may fall—with a given probability—for a certain estimate. These limits may be determined by regression techniques or by examining the distribution within vertical ''slices'' of the scatter plot.

Careful judgment must be applied when estimating confidence intervals for multiple-epoch measures such as that shown in Fig. 6. As demonstrated earlier in this paper, variation in the m component of an l,m spectrum only allows us to ''average out'' the minimal orientation error. Variation in hemispherical error (dependent on l spectrum), without gross violation of the stationarity assumption, is necessary for the average of estimates $\hat{A}$ over multiple epochs to converge to A.

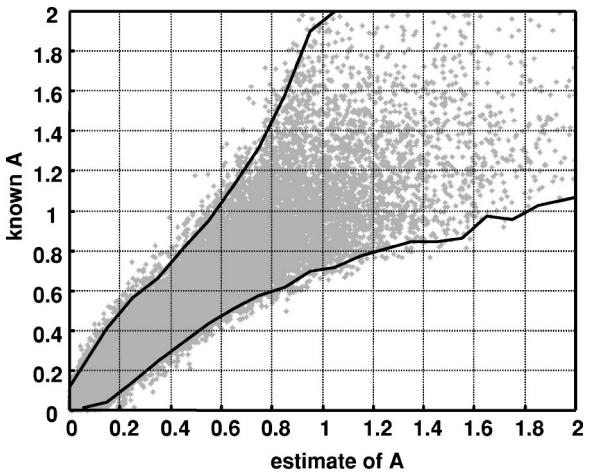

FIG. 8. 95% confidence intervals for single-epoch estimates of the power ratio $A=G_{l=0,1}/G_{l=2\ldots6}$. Twenty thousand potential maps were generated from known, random, realistically distributed (based on genuine EEG data) l spectra, and decomposed using 131 channels and the adjoint harmonic method. Here, known A are plotted against the resulting estimated A. Solid lines indicate the empirical 95% confidence interval for a given estimate of A. Multiple-epoch estimates will result in much smaller intervals, depending on the variation in l spectra being decomposed.

VII. DISCUSSION

Our simulations provide a firm basis for application of spherical harmonic decomposition to irregularly sampled, hemispherical data such as EEG. Our hemispherical modification of Misner's adjoint harmonic method [10] proved most consistent. However, for physiological data of known power distribution, the spline method [9] is complementary and may be slightly more accurate with high-density sampling. It seems that, within the conservative bandlimit of equation [3] and the known spatial filter properties of the head [14], decomposition accuracy will not be materially improved by more than 131 electrodes for scalp EEG. We suggest that confidence intervals for such decompositions, or for decomposition-derived measures, be determined empirically using randomized data. Furthermore, while single-decomposition errors are relatively large, with multiple epochs the experimental accuracy may be increased substantially. For this averaging to be both valid and effective, we must assume a quasistationary wave-number spectrum across our epochs, but with sufficient random variation in hemispherical error for our estimates to converge upon the mean. In addition, especially in EEG applications, we must remain aware of the limitations inherent in collapse across m's (we assume the orientation of the underlying cerebral hemispheres is irrelevant) and the use of spherical harmonics on a hemispheroidal surface.

The dynamical properties of human EEG rhythms are

quite complicated, varying substantially between individuals and brain states. Furthermore, physiologically based theoretical models point to substantial nonlinear effects and interactions across spatial scales [2,24–27]. Despite all the obvious complications, results from the spherical harmonic decomposition of experimental EEG agreed qualitatively with crude linear electrode array results [1,22]. These results were seen in all subjects and are consistent with a mixed global/local model of cortical dynamics, in which lower global-mode oscillations produce alpha rhythm, superimposed on local or spatially uncorrelated activity in various frequency bands [2]. Further study of spatiotemporal EEG dynamics, using spherical harmonic decomposition, should shed more light on these issues.

ACKNOWLEDGMENTS

This work was supported by the Australian Research Council through Grant No. A10019013 and by the U.S. National Science Foundation (B.M.W.).

APPENDIX: ADJOINT HARMONIC METHOD

The fundamental development of Misner's adjoint harmonic method may be found in [10]. Here, we summarize its adaptation to hemispherically sampled data, in notation consistent with the previous sections. We use the real spherical harmonics

$$Y_{lm}(\theta,\phi)=\sqrt{\frac{(2l+1)}{4\pi}\frac{(l-|m|)}{(l+|m|)}}P_l^{|m|}(\cos\theta)\Phi_m(\phi), \tag{A1}$$

where

$$\Phi_m(\phi)=\begin{cases}1 & m=0,\\ \sqrt{2}\cos m\phi & m>0,\\ \sqrt{2}\sin -m\phi & m<0.\end{cases} \tag{A2}$$

The orthogonality relationship of the spherical harmonics Y_A may be discretized over a set of real (Γ) and antipodal (Γ') electrode positions:

$$\langle Y_A|Y_B\rangle=\sum_{x\in(\Gamma\cup\Gamma')}Y_AY_Bw_x. \tag{A3}$$

The electrode weights w_x represent the fraction of scalp area assigned to each electrode, and in our implementation are derived from the mean distance k_x between an electrode x and its three nearest neighbors

$$w_x=4\pi R^2\frac{{k_x}^2}{\sum_{x\in\Gamma}{k_x}^2}. \tag{A4}$$

Note that, if we use solely the hemispherical sample positions Γ in Eq. (A3), the matrix of G_{AB} obtained later is ill conditioned ($R>10^8$) and thus, the G_{AB} cannot be reliably found. In other words, as one might expect, the hemispherical error is not an artifact of discretization, and thus, is not minimizable by the regularization process described here. Rather, the electrode positions are reflected over the horizontal plane to create a set of antipodal positions Γ', and the discretization of Eqs. (A3) and (4) is calculated over the full-sphere set ($\Gamma\cup\Gamma'$).

The matrix of G_{AB}, whose deviation from an identity matrix represents the error introduced by discretization, is thus calculated using Eq. (4). The adjoint harmonics Y^{lm} are obtained from Eq. (6), and used in Eq. (5) to calculate deconvolution coefficients μ_{lm}. The rows of $\boldsymbol{\mu}$ representing antipodal electrode positions are discarded; the remaining μ_{lm} may be used in Eq. (3) to estimate Φ_{lm}. The angular power-spectrum estimate $\hat{G}(l)$ may be calculated from Eq. (12).

[1] P. L. Nunez, *Electric Fields of the Brain: The Neurophysics of EEG* (Oxford University Press, New York, 1981).
[2] P. L. Nunez, *Neocortical Dynamics and Human EEG Rhythms* (Oxford University Press, New York, 1995).
[3] F. H. Lopes da Silva, in *Neocortical Dynamics and Human EEG Rhythms*, edited by P. L. Nunez (Oxford University Press, New York, 1995).
[4] K. E. Misulis, *Essentials of Clinical Neurophysiology* (Butterworth-Heinemann, Boston, 1997).
[5] W. Klimesch, Brain Res. Brain Res. Rev. **29**, 169 (1999).
[6] P. L. Nunez *et al.*, Electroencephalogr. Clin. Neurophysiol. **103**, 516 (1997).
[7] P. Tass *et al.*, Phys. Rev. Lett. **81**, 3291 (1998).
[8] P. L. Nunez, B. M. Wingeier, and R. B. Silberstein (unpublished).
[9] P. J. Cadusch, W. Breckon, and R. B. Silberstein, Brain Topogr **5**, 59 (1992).
[10] C. W. Misner, http://xxx.lanl.gov/abs/gr-qc/9910044, 1999.
[11] M. Boas, *Mathematical Methods in the Physical Sciences* (Wiley, New York, 1983), p. 568.
[12] J. J. Koenderink, A. J. van Doorn, and M. Stavridi, in *Lecture Notes in Computer Science*, Vol. 1065, Proceedings of the Fourth European Conference on Computer Vision, Cambridge, UK, edited by B. Buxton and R. Cipolla (Springer Verlag, Berlin, 1996).
[13] J. S. Bendat and A. G. Piersol, *Random Data* (Wiley, New York, 1986).
[14] R. Srinivasan, P. L. Nunez, D. M. Tucker, R. B. Silberstein, and P. J. Cadusch, Brain Topogr **8**, 355 (1996).
[15] P. J. E. Peebles, Astrophys. J. **185**, 413 (1973).
[16] S. K. Law and P. L. Nunez, Brain Topogr **3**, 365 (1991).
[17] G. C. K. Yeh and J. Martinek, Ann. N.Y. Acad. Sci. **67**, 1003 (1957).
[18] B. N. Cuffin and D. Cohen, IEEE Trans. Biomed. Eng. **24**, 372 (1977).

[19] J. C. de Munck, J. Appl. Phys. **64**, 464 (1988).
[20] P. L. Nunez, Math. Biosci. **21**, 279 (1974).
[21] P. L. Nunez, IEEE Trans. Biomed. Eng. **21**, 473 (1974).
[22] G. R. Shaw, Ph.D. thesis, University of Alberta, 1991.
[23] E. S. Edgington, *Randomization Tests* (Marcel Dekker, New York, 1987).
[24] V. K. Jirsa and H. Haken, Physica D **99**, 503 (1997).
[25] V. K. Jirsa, R. Friedrich, H. Haken, and J. A. S. Kelso, Biol. Cybern. **71**, 27 (1995).
[26] L. Ingber, Physica D **5**, 83 (1982).
[27] L. Ingber, in *Neocortical Dynamics and Human EEG Rhythms*, edited by P. L. Nunez (Oxford University Press, New York, 1995).